AUTHOR(S): SUN, Y., GUO, J., FERNANDEZ, C., HUANG, J. and PENG, Q.

TITLE: In situ atomic-scale oscillation sublimation of magnesium under CO_2 conditions.

YEAR: 2019

Publisher citation: SUN, Y., GUO, J., FERNANDEZ, C., HUANG, J. and PENG, Q. 2019. In situ atomic-scale oscillation sublimation of magnesium under CO_2 conditions. Langmuir [online], 35(1), pages 300-305. Available from: https://doi.org/10.1021/acs.langmuir.8b03580

OpenAIR citation: SUN, Y., GUO, J., FERNANDEZ, C., HUANG, J. and PENG, Q. 2019. In situ atomic-scale oscillation sublimation of magnesium under CO_2 conditions. Langmuir, 35(1), pages 300-305. Held on OpenAIR [online]. Available from: https://openair.rgu.ac.uk/

LANGMUIR

New Concepts at the Interface: Novel Viewpoints and Interpretations, Theory and Computations

In-Situ Atomic-Scale Oscillation Sublimation of Magnesium under CO2 Condition

Yong Sun, Jianxin Guo, Carlos Fernandez, Jianyu Huang, and Qiuming Peng

Langmuir, **Just Accepted Manuscript** • DOI: 10.1021/acs.langmuir.8b03580 • Publication Date (Web): 10 Dec 2018

In-Situ Atomic-Scale Oscillation Sublimation of Magnesium under CO_2 Condition

Yong Sun[1], Jianxin Guo[2], Carlos Fernandez[3], Jianyu Huang[1], Qiuming Peng*[,1]

[1] *State Key Laboratory of Metastable Materials Science and Technology, Yanshan University, Qinhuangdao, 066004, PR. China.*

[2]*Hebei Provincial Key Lab of Optoelectronic Information Materials, College of Physics Science and Technology, Hebei University, Baoding, 071002, PR China*

[3]*School of Pharmacy and Life Sciences, Robert Gordon University, Aberdeen, AB107GJ, UK*

* Corresponding author. Tel.: +86-335-8057047; fax: +86-335-8074545

E-mail address: pengqiuming@ysu.edu.cn

Abstract

Understanding the interactive role between Mg and CO_2 is crucial for many technological applications, including CO_2 storage, melting protection, corrosion resistance and ceramic welding. Here we report observations of rapid oscillation sublimation of Mg at room temperature in the presence of both CO_2 gas and electron irradiation using environmental transmission electron microscopy. The sublimation is mainly related to phase transformation of amorphous $MgCO_3$. Differing from the direct formation of gas-state $MgCO_3$ which attributes to the sublimation of pure Mg under a mild electron beam dose, a unique oscillation process is detected during the process of Mg sublimation under a harsh electron beam dose. The main reason stems from the first-order reaction of a reversible decomposition-formation of amorphous $MgCO_3$. These atomic-level results provide some interesting insights into the interactive role between Mg and CO_2 under electron beam irradiation.

KEYWORDS: Magnesium; Sublimation; Phase transformation; Oscillation

Introduction

As one of active metals, the role between magnesium and gas is an inevitable issue, proventing the development and service of Mg-based materials. Especially, the interactive role between Mg and CO_2 is of importance to control functions in mangy industrial applications, such as CO_2 storage,[1] metal-air batteries,[2] melting protection,[3] corrosion resistance[4] and ceramic welding.[5] Sublimation, as a fundamental chemical-physical phenomenon, is an intense endothermic phase transition between solid and vapor along with chemical reactions, in which the atoms break away from their neighbors in the crystal lattice and then they are removed into gas phase.[6] Interpreting the sublimation mechanism of Mg under CO_2 condition may have a great influence on above-mentioned applications from the scientific interest in combination of the viewpoints of industry. Nevertheless, the majority of previous investigations relative to the sublimation of Mg focused on the equilibrium thermodynamic parameters (enthalpy, vapor pressure, free energy),[7] the kinetics of vaporization in Mg alloys [8], and the observation under a simple oxygen condition.[9] The direct experimental results on this sublimation process are scarce so far owing to high reaction activity and severe reaction temperatures.

To probe the interactive role between gas and metals, researchers have developed several different methods- such as scanning microscopy observation,[10] ambient pressure X-ray photoelectron spectroscopy[11] and *in-situ* environmental transmission electron microscopy (ETEM).[12] Differing from conventional techniques, ETEM that has been evolved recently offers the capability for temperature-, time-, and pressure-resolved

imaging of the interactive role between gas/vapour and a solid, as well as the surface/subsurface layers of materials by introducing a reactive gas to the sample while simultaneously monitoring the structural evolution at the atomic level [13-15]. It provides a unique, important route to look into the spatial details of chemical reaction. Herein, by performing a gas flow of CO_2 and *in situ* ETEM, we firstly investigated the influence of both CO_2 and electron-beam (e-beam) irradiation on the sublimation behavior of Mg in terms of e-beam dose, gas flow rate and kinetics process.

Results and discussion

In-situ sublimation of Mg under CO_2 irradiation condition

To probe the sublimation of pure Mg under CO_2 irradiation environments, a high purity Mg ingot has been prepared by our chill-casting method.[16] The Mg slice along $[1\bar{2}1\bar{3}]$ which was prepared by means of a focus ion beam cutting was selected to identify phase transformation. Unpredictably, when a gas flow of CO_2 was charged, a severe sublimation phenomenon was detected at room temperature under e-beam irradiation. Moreover, as shown in **Figure 1a**, a new hierarchical structure is observed in the front of sublimation edge. The core is crystal Mg, confirmed by selected area fast Fourier transformation (FFT) pattern along the $[1\bar{2}13]$ direction (**Figure 1b**). The separated islands near to pure Mg are assigned to MgO in terms of FFT pattern (**Figure 1c**). The orientation relationship (ORs) between Mg and MgO have been confirmed by the high revolution transmission electron microscopy (**HRTEM, Figure 1b**), wherein the OR is $(0\bar{1}11)_{Mg}||(020)_{MgO}$. This OR is akin to the oxidation behavior of pure Mg under high pure hydrogen condition,[17] but it is

different from that observed results in the high-temperature oxidation, i.e., $(11\bar{2}0)_{Mg}||(220)_{MgO}$ and $[2\bar{1}\bar{1}0]_{Mg}||[001]_{MgO}$,[18] and the low-temperature confined growth of MgO, i.e., $(0002)_{Mg}||(110)_{MgO}$ and $[2\bar{1}\bar{1}0]_{Mg}||[001]_{MgO}$.[19] In addition, the *in-situ* observation results (**Movie 1**) reveal that an amorphous layer with a thickness of ~8 nm is detected on the surface of the sample. With increasing the sublimation time, the interface shrinks rapidly, but the thickness of the amorphous layer remains relatively stable. Attractively, this severe sublimation phenomenon only occurs with the coexistence of CO_2 gas and e-beam irradiation. Specifically, a number of squared-like MgO particles are observed in the sample by adding e-beam irradiation without CO_2 (**Figure S1a**), which might be related to the adsorptive oxygen during sample preparation.[20] In contrast, some Morie fringes and a lot of MgO phases are observed can be detected with the CO_2 gas (under a beam-blanking mode, **Figure S1b**), which is ascribe to the high chemical activity of Mg. Therefore, it can be confirmed that both CO_2 gas and e-beam irradiation are the prerequisites for the rapid sublimation of pure Mg.

To further identify the phase composition on the unique hierarchical structure, both electron energy loss spectroscopy (EELS) and *in-situ* selected area electron diffraction (SAED) have been performed. The low-loss and core-loss of EELS results (**Figure 2a,b**) show that the core and the medium layers are mainly composed of Mg (23.5 eV) and MgO (11.3, 22.6 and 534.2 eV), respectively, which are consistent with the FFT patterns. Comparatively, the amorphous layer is mainly contains of Mg, C and O, which might be associated with $MgCO_3$. This same amorphous phase has also confirmed in ceramic nanowelding of MgO under CO_2 gas.[5] The phase transformation during the reaction process

has been confirmed by *in-situ* SAED. The results (**Figure 2c-e**) demonstrate that the Mg firstly changes into crystalline MgO, and then the MgO varies into amorphous $MgCO_3$.

Effect of e-beam doses on sublimation of Mg

To probe the effect of e-beam doses on the sublimation of Mg, the sublimation processes of Mg under different e-beam doses have been investigated. In the case of a mild dose e-beam of 5×10^4 e/nm^2·s, the hierarchical structure formed in the initial stage, and then the structure maintains stable (**Movie 2**). With retarding the irradiation time, the whole interface shrinks continuously, but the surface contour of the sample remains invariable. In addition, except for the Mg, MgO and $MgCO_3$, there are some droplets on the surface, which is confirmed as amorphous graphite-carbon, in terms of EELS result (**Figure 2a**). This result is consistent with the calcination mechanism of Mg under CO_2 condition.[21] Time-lapse images show (**Figure 3a-d**) that some cracks forms on the surface of the sample with increasing the irradiation time. The maximum sublimation rate (based on the variation distance of the sublimation tip) is ~1 nm·s^{-1}. Meanwhile, some quadrate-like particles are detected near to the tip of sublimation edge. Both of them are related to the presence of MgO phases, in which the large stress between the interface of Mg and MgO results in the formation of cracks.[22]

In contrast, the surface changes into more active with increasing the e-beam dose to 1×10^5 e/nm^2·s (**Figure 3c-f**, **Movie 3**). On the one hand, the exterior amorphous layer slightly shinks with retarding irradiation time, analogous to the sublimation of Mg under a mild e-beam dose. On the other hand, some bubbles are detected near to the amorphous layer. These bubbles were observed to oscillate continuously, with both inflation and

deflation of the bubble dimension with time. The maximum sublimation rate increases to ~1.8 nm·s^{-1}. Furthermore, it is worthy note that some dot-shaped particles were observed after oscillation, and its number increases dependent on the oscillation frequency. The HRTEM image (**Figure S2**) shows that the nano dot-like particle is assigned to crystalline MgO, with a dimension of ~15 nm. The different OR between adjacent MgO particles indicates that they form discontinuously.

More interestingly, the bubbles cover on the whole surface of the sample under a harsh e-beam dose of 7×10^5 e/nm^2·s (**Figure 4a-d**). Both inflation and deflation of the bubble size varies dependent on the time (**Movie 4**). The effect of CO_2 pressure and electron dose on the frequency and amplitude of the oscillatory motion has been investigated. The variation in the diameter of the largest bubble was measured over time to obtain the amplitude and frequency at different pressures and electron doses. Specifically, when the CO_2 gas pressure was increased, the frequency of the structural oscillations and the amplitude (~210 nm) changed slightly (**Figure 4e, Movies 4, 5**). The possible reason is that the fluctuation of gas flow is slight owing to the limitation of the instrument, wherein a large gas flow results in the vibration of sample and gas leakage. Comparatively, an increment in e-beam irradiation results in increased oscillation frequency and decreased oscillation amplitude. At a constant CO_2 pressure of 1.0 mbar, the increment of the electron dose rate from 1×10^5 e/nm^2·s (**Movie 6**) to 1×10^7 e/nm^2·s (**Movie 7**) resulted in an increase in the oscillation frequency from 0.05 to 0.18 Hz, while the maximum displacement decreased from 42 to 21 nm (**Figure 4f**).

Oscillation sublimation mechanism

The reaction process demonstrates that oscillation phenomenon is related to e-beam and CO_2. The oscillatory motion suggests that the stretched bubble surface can recover after shrinking, which may be related to the high mobility of gas ions which can re-adsorb the CO_2 to re-inflate the bubbles. This process is also similar to hydrogen generation and storage in $NaBH_4$ compounds, which provides as the new method for hydrogen-energy process chain and hydrogen economics.[23-25]

Taking a single bubble as an example (**Figure S4)**, a simple model can be performed to describe the above oscillation process (**Figure 4g**).[26] The interior of bubble is an isolated environment, and the gas can be treated as an ideal gas. Thus, we will have:

$$p_{\mathrm{b}}V = nR\mathrm{T} \quad (1)$$

where p_{b} is the pressure inside the bubble, V is the volume of the bubble, n is the mole number of CO_2 gas in the bubble, R is the gas constant, and T is the temperature. In the case of classic bubbles:

$$p_{\mathrm{b}} - p_{\mathrm{T}} = 4S/\mathrm{d} \quad (2)$$

where p is the pressure in TEM, S is the surface energy of $MgCO_3$, and d is the bubble size (bubble diameter). Here $p_b \gg p_T$ due to the low pressure in TEM and high pressure in bubble to cause $MgCO_3$ deformation. Therefore:

$$p_b \approx 4S/\mathrm{d} \quad (3)$$

Combine (1) and (3), notice that $V = \pi \mathrm{d}^3/6$, we have:

$$n \approx 2\pi S\mathrm{d}^2/3R\mathrm{T} \quad (4)$$

This implies us:

$$n \propto \mathrm{d}^2 \quad (5)$$

During inflation and deflation processes, if we assume gas evolution and oxygen leaking are the rate-determine steps, respectively, then:

For inflation process: $\Delta(n) = \alpha_{ger}\,\Delta(t)$ (6)

For deflation process: $\Delta(n) = \beta_{glr}\,\Delta(t)$ (7)

where t is the time, α_{ger} is the gas evolution rate, and β_{glr} is the oxygen leaking rate. For the first-order approximation, if we treat the rates of gas evolution and leaking as constants, from (5), (6) and (7) we can get:

$\Delta(d^2) \propto \Delta(t)$ (8)

With these approximations, the relationship of $\Delta(d^2) \propto \Delta(t)$ can be inferred. This relationship can also be proofed by plotting the square of bubble size (d^2) against time. It implies that the oscillation process is related to a reversible first-order reaction.[27] Moreover, further testing confirms that the double bubbles also agree the first-order reaction in terms of linear trends dependent on two different stages (**Figure S5**). When the bubbles grow to larger sizes and the thickness of their skin reduces below some critical thickness (the order of 1~2 nm, **Movie 4**), the gas molecules inside will begin to leak away and start the deflation process. However, CO_2 gas was activated under harsh dose e-beam irradiation, experimentally composing of CO^{2+}, CO^{+}, CO, O^{+}, O^{2+} *etc*.[28] Therefore, additional studies are required to identify the ionc composition during the oscillation in the future.

As a result, as illustrated in **Figure 5**, the whole sublimation of pure Mg under CO_2 irradiation condition can be divided into three stages:

The first stage:

$Mg(s)+CO_2(s) \rightarrow MgO(s) + C(s)$ (9)

The second stage can be shown as:

$$MgO(s)+CO_2\ (g)\leftrightarrow MgCO_3\,(s,\ amorphous) \quad (10)$$

The third stage can be divided into two types of sublimation depending on e-beam doses:

$$\text{Type I: } MgCO_3\ (s,\ amorphous) \rightarrow MgCO_3\,(g) \quad \text{(under a mild e-beam dose)} \quad (11)$$

$$\text{Type II: } MgCO_3\ (s) \leftrightarrow MgO\ (s) + CO_2\ (g) \quad \text{(under a harsh e-beam dose)} \quad (12)$$

Note that the accelerated sublimation of Mg under CO_2 irradiation condition occurs at room temperature. According to the *Clapeyron-Clausius* equation,[29] the boiling temperature (**Eq. 3**) and decomposed temperature (**Eq. 4**) reduce remarkably since the exterior gas pressure is reduced. For instance, the decomposition temperature of $MgCO_3$ changes from ~350 to ~170 ^oC in the case of CO_2 gas pressure of 0.1 mbar. Thus, the concentrated e-beam can achieve this reaction without external heat source.

In addition, the disappearance of grahite-carbon might be related to the following chemical reaction:

$$C(s)+CO_2\ (g \rightarrow 2CO\ (g) \quad (13)$$

Unfortunately, it is impossible to identify the prescence of CO gas under ETEM observation owing to the similar elemental composition and complex ionics compositions. Note that this possible chemical reaction mainly occurs in the surface of C without forming the bubbles. More imporatnly, given that the CO_2 penetrates the surface of C, the mole amount of gas remains invariable, and the oscillation would never occur. Therefore, the CO_2 gas instead of CO gas accounts for the oscillation process.

Conclusions

In-situ ETEM observations have been performed to investigate the unique sublimation of

Mg under CO_2 irradiation condition. Differing from the oxidation of Mg, severe sublimation phenomenon is detected due to the coexistence of electron irradiation and CO_2. The fundamental reason is related to the formation of amorphous $MgCO_3$. The direct sublimation of $MgCO_3$ phase accounts for the continuous sublimation of pure Mg under a mild electron dose. In turn, the decomposition of amorphous $MgCO_3$ plays a crucial role in accelerating the sublimation of Mg under a harsh electron dose, resulting in a unique oscillatory phenomenon. The reason for oscillation stems from the first-order reversible phase transformation of $MgCO_3$. These observations provide a thorough understanding of the interactive role between Mg and CO_2 under e-beam irradiation, and point towards new routes in the design of Mg materials with enhanced anti-corrosion and welding properties under CO_2 condition.

Experimental procedure

High purity Mg (>99.9%) ingot was melted at 720 ^oC for 1 h, and then directly solidified by a chill-casting method. The cooling rate was below 0.5 mm/s to achieve the bar of 50 mm in diameter with a large grain size (~ 5 mm). The grain orientation was confirmed by electron back scattered diffraction equipped with a HKL-EBSD system. The specimens were prepared by traditional mechanical grinding and polishing from 500 to 10 μm in thickness, then ion-beam milling using Gatan PIPS 691 with 4 keV. The atomic structures of specimens were identified by high revolution transmission electron microscopy (HRTEM, FEI TITAN ETEM G2: an ultra-high point resolution of 0.1 nm with a Gatan Model-994 CCD digital camera and an electron energy loss spectrometer (EELS), operated

at a voltage of 300 kV. The CO_2 gas around the thin specimen was performed at a pressure range of 0.5 ~ 1.2 mbar during the entire experiments, and the range of e-beam dose is between 5×10^3 and 1×10^7 e/nm^2·s. Video and image recording were started only until the range of pressure of dioxide-gas was reached.

Supporting Information Available

Additional figures and movies as described in the text. This material is available free of charge via the Internet.

Acknowledgements

We greatly acknowledge the financial support from National Key Research and Development Program (2017YFB0702001), National Natural Science Foundation-Outstanding Youth Foundation (51771162). and the Natural Science Foundation of Hebei Province (E2017201034).

References

(1) Kelemen, P. B.; Matter, J. *In situ* carbonation of peridotite for CO_2 storage. *Proc. Natl. Acad. Sci.* **2008,** *105,* 17295-17300.

(2) Zhang, X.; Wang, X.G.; Xie, Z.; Zhou, Z. Recent progress in rechargeable alkali metal–air batteries. *Green Energy Environ.* **2016,** *1*, 4-17.

(3) Yang, S. C.; Lin, Y. C. Magnesium alloy melt protection by high-efficiency phase transition of carbon dioxide. *J. Clean. Prod.* **2013,** *41,* 74-81.

(4) Wang Y.C., Liu B.Y., Zhao X.A., Zhang X.H., Miao Y.C., Yang B., Zhang L. X., Kuang W.J., Li J., Ma E., Shan Z.W. Turning a native or corroded Mg alloy surface into

an anti-corrosion coating in excited CO_2, *Nat. Commun.***2018**, 9, 4058.

(5) Zhang, L.; Tang, Y.; Peng, Q.; Yang, T.; Liu, Q.; Wang, Y.; Li, Y.; Du, C.; Sun, Y.; Cui, L.; Yang, F.; Shen, T.; Shan, Z.; Huang, J. Ceramic nanowelding. *Nat. Commun.* **2018,** *9,* 96.

(6) Buha, J.; Gaspari, R.; Del Rio Castillo, A. E.; Bonaccorso, F.; Manna, L. Thermal stability and anisotropic sublimation of two-dimensional colloidal Bi_2Te_3 and Bi_2Se_3 nanocrystals. *Nano Lett.* **2016,** *16,* 4217-4223.

(7) Scheidema, M. N.; Taskinen, P. Decomposition thermodynamics of magnesium sulfate. *Ind. Eng. Chem. Res.* **2011,** *50,* 9550-9556.

(8) Czerwinski, F. The early stage oxidation and evaporation of Mg-9%Al-1%Zn alloy. *Corr. Sci.* **2004,** *46,* 377-386.

(9) Yu, Q.; Mao, M. M.; Li, Q. J.; Fu, X. Q.; Tian, H.; Li, J. X.; Mao, S. X.; Zhang, Z. *In situ* observation on dislocation-controlled sublimation of Mg nanoparticles. *Nano Lett.* **2016,** *16,* 1156-1160.

(10) Yamasaki, H.; Yamaguchi, H.; Hattori, K.; Neksa, P. Experimental observation of CO_2 dry-ice behavior in an evaporator/sublimator. *Energy Proc.* **2017,** *143,* 375-380.

(11) Stoerzinger, K. A.; Hong, W. T.; Crumlin, E. J.; Bluhm, H.; Biegalski, M. D.; Shao-Horn, Y. Water reactivity on the $LaCoO_3$ (001) surface: An ambient pressure x-ray photoelectron spectroscopy study. *J. Phys. Chem. C* **2014,** *118,* 19733-19741.

(12) Zou, L.; Li, J.; Zakharov, D.; Stach, E. A.; Zhou, G. *In situ* atomic-scale imaging of the metal/oxide interfacial transformation. *Nat. Commun.* **2017,** *8,* 307.

(13) Chou, Y. C.; Wu, W. W.; Cheng, S. L.; Yoo, B. Y.; Myung, N.; Chen, L. J.; Tu, K. N.

In-situ TEM observation of repeating events of nucleation in epitaxial growth of nano $CoSi_2$ in nanowires of Si. *Nano Lett.* **2008,** *8,* 2194-2199.

(14) Nielsen, M. H.; Aloni, S.; De Yoreo, J. J. *In situ* TEM imaging of $CaCO_3$ nucleation reveals coexistence of direct and indirect pathways. *Science* **2014,** *345,* 1158-1162.

(15) McDowell, M. T.; Lee, S. W.; Harris, J. T.; Korgel, B. A.; Wang, C.; Nix, W. D.; Cui, Y. *In situ* TEM of two-phase lithiation of amorphous silicon nanospheres. *Nano Lett.* **2013,** *13,* 758-764.

(16) Peng, Q.; Huang, Y.; Zhou, L.; Hort, N.; Kainer, K. U. Preparation and properties of high purity Mg-Y biomaterials. *Biomaterials* **2010,** *31,* 398-403.

(17) Peng, Q.; Sun, Y.; Ge, B.; Feng, J.; Guo, J.; Fernandez, C.; Huang, J. *In-situ* atomic-scale phase transformation of Mg under hydrogen conditions. *J. Phys. Chem. C* **2018,** *122,* 19532-19539.

(18) Kooi, B. J.; Palasantzas, G.; Hosson, J. T. M. D. Gas-phase synthesis of magnesium nanoparticles: A high-resolution transmission electron microscopy study. *Appl. Phys. Lett.* **2006,** *89,* 161914.

(19) Zheng, H.; Wu, S.; Sheng, H.; Liu, C.; Liu, Y.; Cao, F.; Zhou, Z.; Zhao, X.; Zhao, D.; Wang, J. Direct atomic-scale observation of layer-by-layer oxide growth during magnesium oxidation. *Appl. Phys. Lett.* **2014,** *104,* 141906.

(20) Cao, F.; Zheng, H.; Jia, S.; Liu, H.; Li, L.; Chen, B.; Liu, X.; Wu, S.; Sheng, H.; Xing, R.; Zhao, D.; Wang, J. Atomistic observation of structural evolution during magnesium oxide growth. *J. Phys.Chem. C* **2016,** *120,* 26873-26878.

(21) Hu, X.; Li, Z.; Zhao, Y.; Sun, J.; Zhao, Q.; Wang, J.; Tao, Z.; Chen, J. Quasi–solid

state rechargeable Na-CO_2 batteries with reduced graphene oxide Na anodes. *Sci. Adv.* **2017,** *3*. e1602396

(22) Xu, W.; Horsfield, A. P.; Wearing, D.; Lee, P. D. Diversification of MgO//Mg interfacial crystal orientations during oxidation: A density functional theory study. *J. Alloys Compd.* **2016,** *688,* 1233-1240.

(23) Ouyang, L.Z; Chen, W.; Liu, J.; Felderhoff, M; Wang, H.; Zhu, M. Enhancing the regeneration process of consumed NaBH4 for hydrogen storage. *Adv. Energy Mater.* **2017,** 7, 1700299.

(24) Chen, W.; Ouyang, L. Z.; Liu, J. W.; Yao, X. D.; Wang, H.; Liu, Z. W.; Zhu, M. Hydrolysis and regeneration of sodium borohydride (NaBH4) – A combination of hydrogen production and storage. *J. Power Sources* **2017**, 359, 400-407.

(25) Zhong, H.; Ouyang, L. Z.;Ye, J. S.; Liu, J. W.; Wang, H.; Yao, X.; Zhu, M. An one-step approach towards hydrogen production and storage through regeneration of $NaBH_4$. *Energy Storage Mater.* **2017**, 7, 222–228.

(26) Han, B.; Stoerzinger, Kelsey A.; Tileli, V.; Gamalski, Andrew D.; Stach, Eric A.; Shao-Horn, Y. Nanoscale structural oscillations in perovskite oxides induced by oxygen evolution. *Nat. Mater.* **2016,** *16,* 121.

(27) Sahu, H.; Mohanty, K. Pseudo-first order reaction kinetics and thermodynamic properties study of neem oil esterification using MgO grafted natural hydroxyapatite. *RSC Adv.* **2016,** *6,* 8892-8901.

(28)Willis, C.; Boyd, A. W.; Bindner, P. E. Carbon monoxide yields in the radiolysis of carbon dioxide at very high dose rates. *Can. J. Chem.* **1970,** 48, 1951-1954.

(29) Reid, R. C. P., J. M.; Poling, B. E. , *The Properties of Gases & Liquids*. McGraw-Hill: New York, 1987.

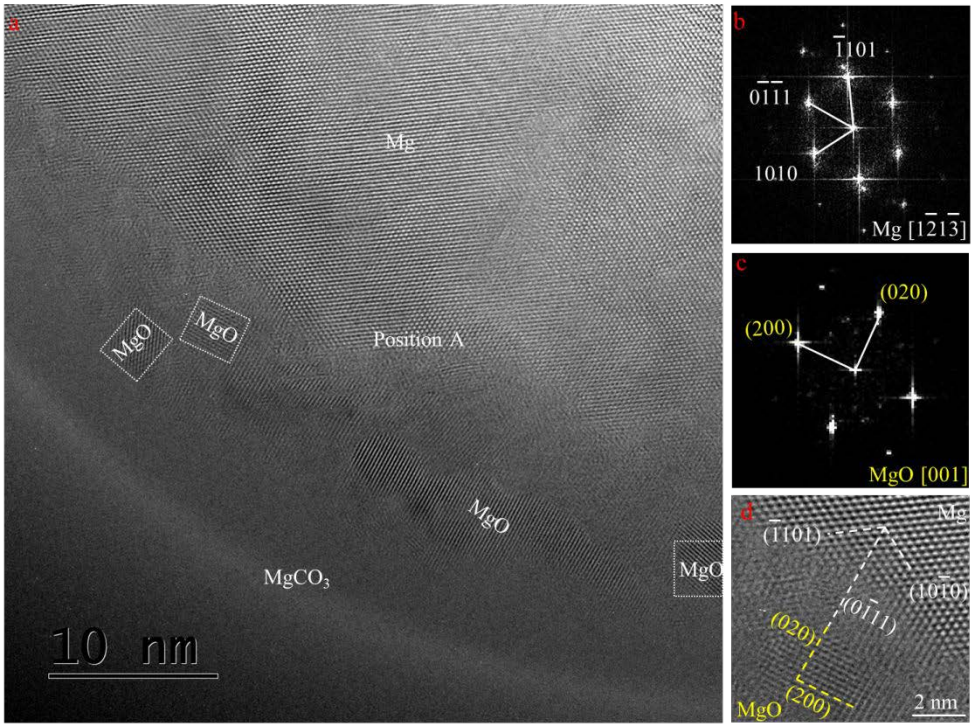

Figure 1. **Sublimation characteristics of pure Mg under CO_2 irradiation.** (a) Typical HRTEM image of the sublimation edge containing different phases. (b) Selected area FFT pattern of the Mg core. (c) Selected area FFT pattern of the MgO layer. (d) Typical HRTEM image of the interface between Mg and MgO, confirming the orientation relationship between Mg and MgO: $(0\bar{1}11)_{Mg}||(020)_{MgO}$.

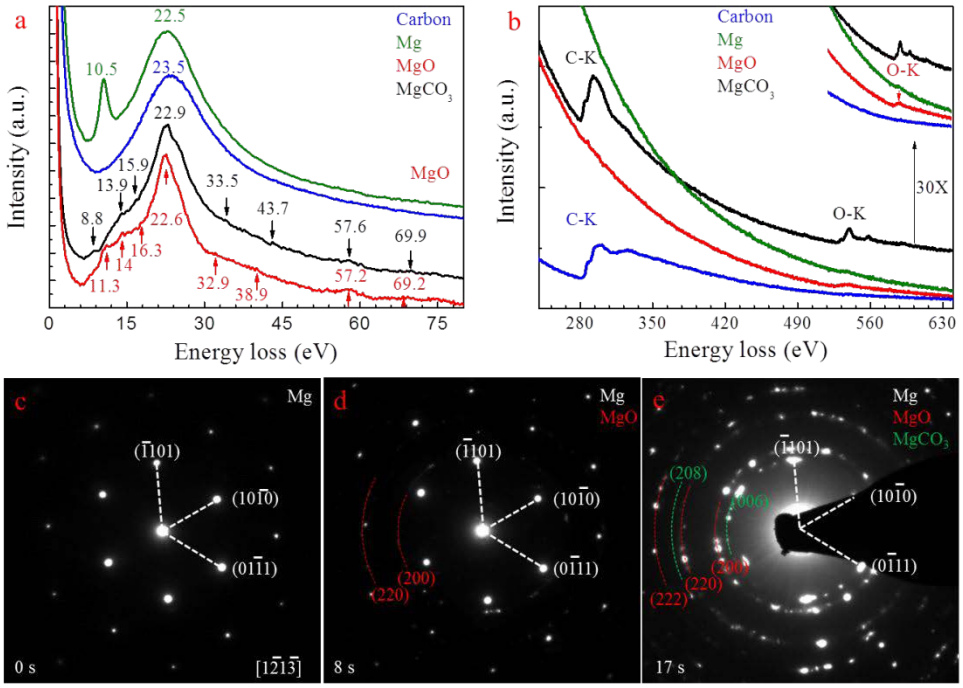

Figure 2. **Phase composition and evolution.** EELS profiles of different phases during sublimation process: (a) low-loss profiles, (b) core-loss profiles, respectively. Mg, MgO and $MgCO_3$ are confirmed in terms of Fig.1a, and C is identified dependent on Fig.3a. (c-e) *In-situ* SAED patterns of phase transformation of the position A in Fig.1a.

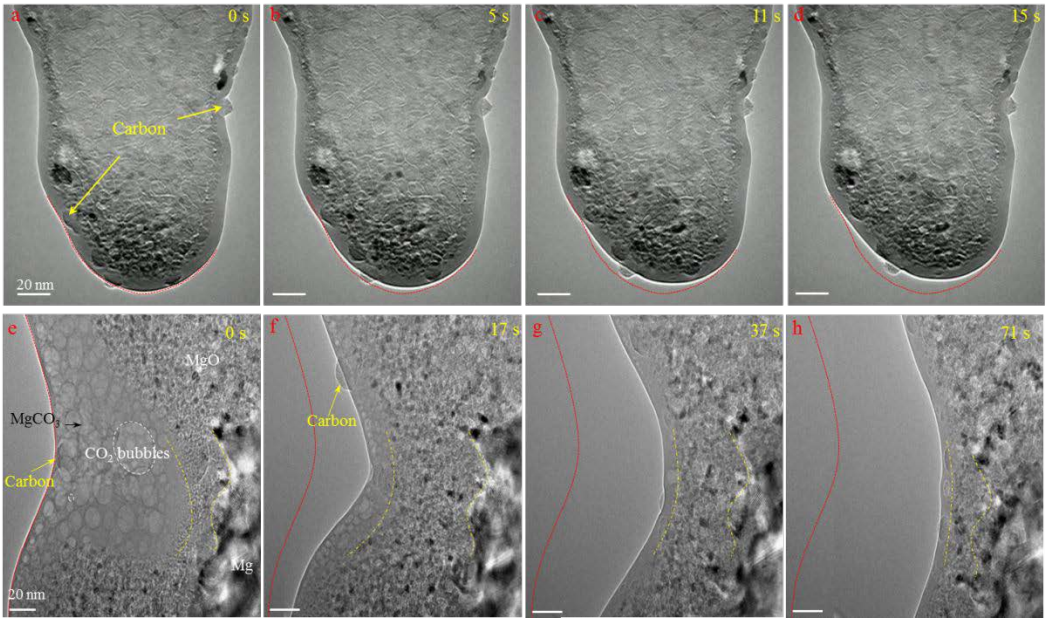

Figure 3. **Effect of e-beam doses on sublimation process.** (a-d) Time-lapse TEM images under a mild e-beam dose of 5×10^3 e/nm^2·s under a CO_2 pressure of 0.5 mbar. The amorphous layer direct sublimates during the reaction process without bubbles. The fluid in the substrate surface is carbon in terms of EELS. (e-h) Time-lapse TEM images under a medium e-beam dose of 1×10^5 e^4/nm^2·s under a CO_2 pressure of 0.5 mbar. Both direct sublimation of the amorphous $MgCO_3$ layer and the bubbles occur simultaneously. The surface is dominated by direct sublimation, but the interior is ascribed to phase decomposition.

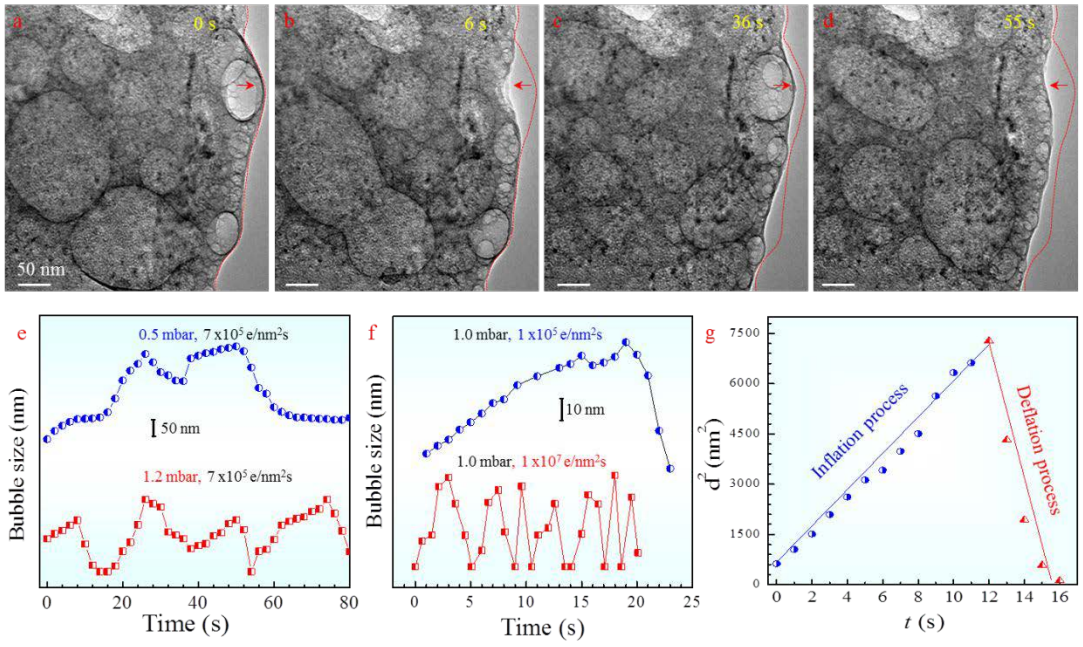

Figure 4. Sublimation process under a harsh e-beam dose. (a-d) Time-lapse TEM images under a harsh e-beam dose of 7×10^5 e/nm^2·s under a CO_2 pressure of 0.5 mbar. (e) Bubble size (the max diameter) evolution over time in the presence of an electron dose rate of 7×10^5 e/nm^2·s and a CO_2 pressure of 0.1 and 1.2 mbar. (f) Bubble size evolution over time in the presence of 1.0 mbar CO_2 pressure and an electron dose rate of 1×10^5 and 1×10^7 e/nm^2·s. (g) Plot of the square of the bubble size (d^2) versus the time (t) during the first inflation process (circle) and the first deflation process (triangle) (data points from Fig. S4). The lines are a linear fit of the inflation and deflation processes.

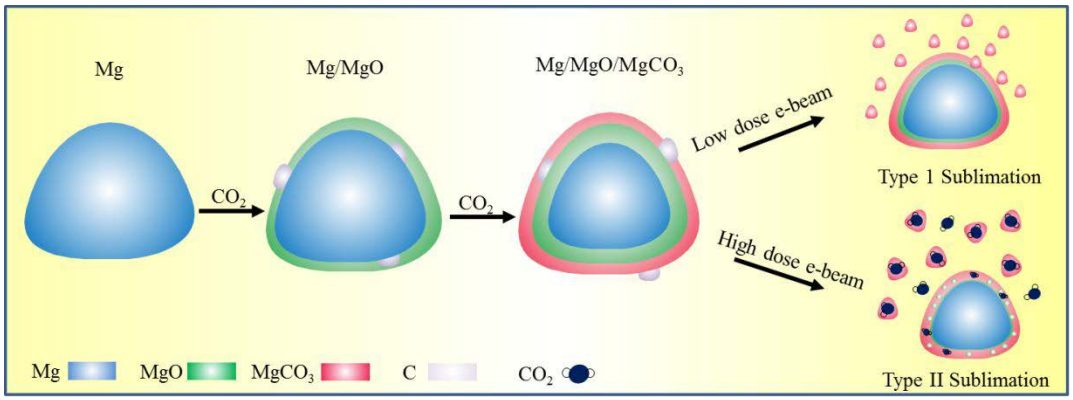

Figure 5. Sublimation mechanisms. The sublimation of Mg under CO_2 irradiation conditions mainly involves two different routes. The direct sublimation of amorphous $MgCO_3$ ($MgCO_3(s) \rightarrow MgCO_3(g)$) plays a dominative role in accelerating sublimation of pure Mg under a mild e-beam condition (a lower temperature). In contrast, the decomposition of amorphous $MgCO_3$ ($MgCO_3(s) \leftrightarrow MgO(s)+CO_2(g)$) chiefly accounts for the rapid sublimation of pure Mg under a harsh e-beam condition (a higher temperature).

Table of content

A rapid sublimation of Mg at room temperature in the presence of CO_2 gas and electron irradiation has firstly observed. The main reason is mainly related to phase transformation of amorphous $MgCO_3$. The gas-state $MgCO_3$ directly attributes to the sublimation of pure Mg under a mild electron dose. A unique oscillation motion process which stems from the first-order reversible decomposition of amorphous $MgCO_3$ dominates the sublimation of Mg under a harsh electron dose.